



Kinematic and static analysis of a cable-driven 2-X tensegrity manipulator for two actuation strategies

Vimalesh Muralidharan, Philippe Wenger, Christine Chevallereau

► To cite this version:

Vimalesh Muralidharan, Philippe Wenger, Christine Chevallereau. Kinematic and static analysis of a cable-driven 2-X tensegrity manipulator for two actuation strategies. *Advances in Robot Kinematics* 2022, Jun 2022, Bilbao, Spain. hal-03797235

HAL Id: hal-03797235

<https://hal.science/hal-03797235>

Submitted on 4 Oct 2022

HAL is a multi-disciplinary open access archive for the deposit and dissemination of scientific research documents, whether they are published or not. The documents may come from teaching and research institutions in France or abroad, or from public or private research centers.

L'archive ouverte pluridisciplinaire **HAL**, est destinée au dépôt et à la diffusion de documents scientifiques de niveau recherche, publiés ou non, émanant des établissements d'enseignement et de recherche français ou étrangers, des laboratoires publics ou privés.

Kinematic and static analysis of a cable-driven 2-X tensegrity manipulator for two actuation strategies

Vimalesh Muralidharan, Philippe Wenger, and Christine Chevallereau

Laboratoire des Sciences du Numérique de Nantes (LS2N), CNRS, 44321 Nantes, France {Vimalesh.Muralidharan@ls2n.fr, Philippe.Wenger@ls2n.fr, Christine.Chevallereau@ls2n.fr}

Abstract. This paper analyzes the instantaneous kinematic and static performance of a two degree-of-freedom serial manipulator composed of anti-parallelogram (or X-) tensegrity joints and remotely driven with cables. Two actuation schemes with 4 cables and 3 cables, respectively, are considered for this manipulator. The physical limitations on the velocities and forces of the actuating cables are mapped onto the task space of the manipulator, to quantify the corresponding velocity and force-application capabilities of the end-effector. A comparative study is carried out between the 4-cable and 3-cable actuation schemes in terms of their velocity and force performance.

Keywords: Tensegrity manipulator, Anti-parallelogram joint, Velocity kinematics, Static analysis

1 Introduction

Cable-driven parallel robots have gained immense popularity over the past two decades, due to their large workspaces, high payload to weight ratio, and fast dynamics. A vast fraction of literature on these robots has been directed towards the study of their wrench-feasibility [1],[2]. The twist feasibility analysis of such robots has been conducted in [3]. Both wrench and twist capabilities of these robots are usually represented by convex polytopes [2],[3]. Two performance measures, namely, manipulability, and condition index, have been extended from ellipsoids to polytopes in [4]. These measures will be used in this paper.

Unlike cable-driven parallel robots, the literature dedicated to cable-driven serial robots [5] is relatively sparse. A difficult challenge that exists in these robots is to find a suitable cable routing scheme [6]. The force-closure analysis of cable-driven open chains has been performed using reciprocal screw theory in [7]. Most of these papers consider robots composed of simple revolute joints only. As an alternative, it is possible to use an anti-parallelogram joint (referred as X-joint) [8]. The X-joint has been used for modeling bio-mechanical systems such as the knee [9], and inter-vertebrae joints of the bird neck [10]. The kinematic analysis of a 2-X manipulator with link offsets has been performed in [11], where

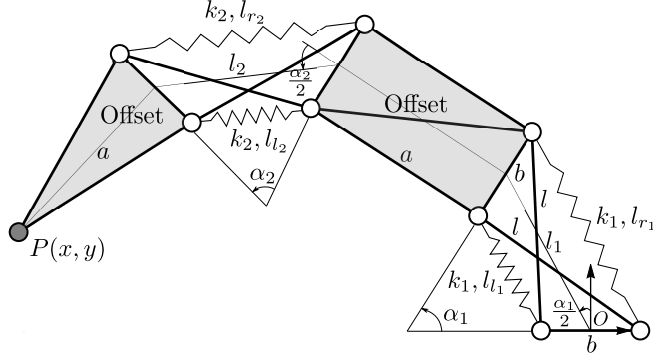


Fig. 1: Schematic of the 2-X tensegrity manipulator with link offsets, $\alpha_i \in]-\pi, \pi[$.

it was shown that this manipulator has a larger workspace than a conventional 2-revolute manipulator with the same maximal reach and joint limits.

This paper studies a two degree-of-freedom (DoF) manipulator composed of two X-joints arranged in series with rigid offsets between them (see Fig. 1). Two different actuation strategies with 4 cables and 3 cables, respectively, are proposed for this manipulator. The 4-cable scheme is a direct extension of the antagonistic actuation of a single X-joint [12] to two of them, while the 3-cable scheme uses the minimum number of cables required to fully actuate this 2-DoF system [7]. One of the objectives of this study is to see the impact of reducing the number of actuators and therefore the cost of the associated robot. It might seem obvious that reducing the number of actuators will reduce the performance of the robot, but we will show that it is not so direct.

In the following, a complete description of the 2-X manipulator, 4-cable and 3-cable actuation schemes are presented. The performance of these two schemes is studied in terms of instantaneous velocity and force transmission. Finally, this performance is compared inside the respective workspaces of the two schemes.

2 Manipulator description and kinematic relations

A schematic of the 2-X manipulator with two X-joints and link offsets is shown in Fig. 1. Each X-joint is composed of a base and top bar of length b and two crossed bars of length l , such that $(l > b)$ for its assembly. Two rigid offsets of length a are introduced between the two X-joints and between the second joint and the end-effector point $P(x, y)$, as shown in the schematic (shaded parts).

For the i^{th} X-joint, the orientation of the top bar relative to its base bar, is given by α_i . This joint is equipped with identical springs of stiffness k_i (zero free-length) on the two sides, ensuring that it remains in equilibrium at $\alpha_i = 0$, in the absence of forces. Since the flat-singularities at $\alpha_i = \pm\pi$ limit the movement of this joint, the study of this manipulator is carried out only for $\alpha_i \in]-\pi, \pi[$, $i = 1, 2$. Within this range, it is possible to unambiguously write the

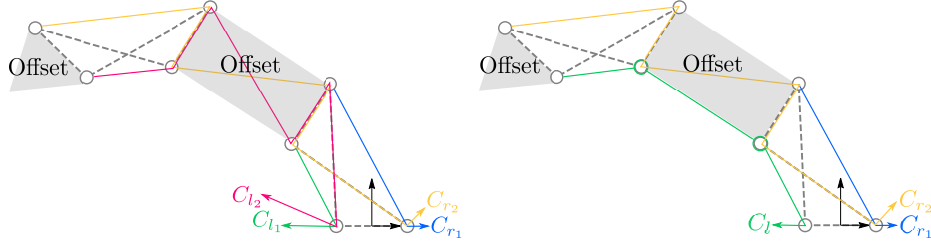


Fig. 2: Actuation scheme with 4 cables (left) and 3 cables (right).

direct kinematics of this manipulator as follows (see [11] for details):

$$\begin{cases} l_i(\alpha_i) = \sqrt{l^2 - b^2 \cos^2(\alpha_i/2)}, & i = 1, 2 \\ x = -l_1(\alpha_1) \sin(\alpha_1/2) - a(\sin \alpha_1 + \sin(\alpha_1 + \alpha_2)) - l_2(\alpha_2) \sin(\alpha_1 + \alpha_2/2) \\ y = l_1(\alpha_1) \cos(\alpha_1/2) + a(\cos \alpha_1 + \cos(\alpha_1 + \alpha_2)) + l_2(\alpha_2) \cos(\alpha_1 + \alpha_2/2) \end{cases} \quad (1)$$

Differentiating the above equations w.r.t. time yields :

$$\begin{bmatrix} \dot{x} \\ \dot{y} \end{bmatrix} = \mathbf{J} \begin{bmatrix} \dot{\alpha}_1 \\ \dot{\alpha}_2 \end{bmatrix}, \mathbf{J} = \begin{bmatrix} \frac{\partial x}{\partial \alpha_1} & \frac{\partial x}{\partial \alpha_2} \\ \frac{\partial y}{\partial \alpha_1} & \frac{\partial y}{\partial \alpha_2} \end{bmatrix} = \begin{bmatrix} J_{11} & J_{12} \\ J_{21} & J_{22} \end{bmatrix}, \text{ is a Jacobian matrix.} \quad (2)$$

The side lengths l_i, l_{r_i} with $i = 1, 2$ (see Fig. 1) can be expressed as follows [10]:

$$\begin{cases} l_i = -b \sin(\alpha_i/2) + \sqrt{l^2 - b^2 \cos^2(\alpha_i/2)} \implies \dot{l}_i = -Z_{l_i} \dot{\alpha}_i \\ l_{r_i} = b \sin(\alpha_i/2) + \sqrt{l^2 - b^2 \cos^2(\alpha_i/2)} \implies \dot{l}_{r_i} = -Z_{r_i} \dot{\alpha}_i, \text{ where,} \\ Z_{l_i} = -\frac{dl_i}{d\alpha_i} = b \cos(\alpha_i/2) \left(1 - \frac{b \sin(\alpha_i/2)}{\sqrt{l^2 - b^2 \cos^2(\alpha_i/2)}} \right) \\ Z_{r_i} = -\frac{dl_{r_i}}{d\alpha_i} = -b \cos(\alpha_i/2) \left(1 + \frac{b \sin(\alpha_i/2)}{\sqrt{l^2 - b^2 \cos^2(\alpha_i/2)}} \right) \end{cases} \quad (3)$$

Note that $Z_{l_i} > 0$ and $Z_{r_i} < 0$ when $l > b$ and $\alpha_i \in]-\pi, \pi[$. The numerical data that will be used in this paper for the purpose of illustration are: $b = 0.05$ m, $l = 0.1$ m, $a = 0.2$ m, $k_1 = 600$ N/m, $k_2 = 300$ N/m. All the bars are assumed to be made of Aluminum material with a circular cross-section of radius 0.005 m.

3 Cable actuation schemes

The 2-X manipulator will be remotely actuated by motors fixed in the base, using cables as transmission elements. Two such actuation schemes are considered in this study. The first one, referred as the 4-cable scheme, involves four actuators/cables (see Fig. 2, left), namely, $C_{l_1}, C_{r_1}, C_{l_2}, C_{r_2}$. The cables C_{l_1} and C_{r_1} actuate the first joint *antagonistically* without any effect on the second one. The other two cables C_{l_2} and C_{r_2} are routed through the rigid links with pulleys,

following the *strut-routed* scheme [8], to actuate the second joint independent of the first one. The advantage of this scheme is the *independence* in actuation of the two joints, but it uses one cable more than the minimum required [7].

The second actuation scheme, referred as the 3-cable scheme, uses only three actuators/cables (see Fig. 2, right), the minimum number required for this system [7]. Cables C_{r_1} and C_{r_2} have the same connections as in the 4-cable scheme. In contrast, the cable C_l is routed along the left side of both the joints in a *side-routed* scheme [10]. It is wound completely around two of the pulleys (at the top left of the first joint and bottom left of the second joint) before being connected to the top left vertex of the second X-joint. This way, the cable C_l can control the movement of both the joints, albeit in a dependent manner.

In this paper, the cables are assumed to be inextensible and the pulleys are approximated as massless points, i.e., with zero radius. The velocity and static force analysis for the two actuation schemes are presented in the following. The velocity analysis is useful for designing robots for manipulation tasks like palletizing, while the force analysis is relevant for machining tasks like drilling.

4 Instantaneous velocity analysis

In a cable-driven system, the peak speed of the cables and the maximum force transmitted by them, are limited by the actuators driving them. The aim of this section and the next one is to map these limitations onto the task space and evaluate the capabilities of the manipulator.

Let us assume that all the cables are actuated by identical motors, the one used in [10]. Using the data sheet of the specified motor and the drum characteristics, a value for maximum cable speed can be found as $\dot{l}_{\max} = 0.423$ m/s. From Fig. 2, it is apparent that the velocities of the cables C_{l_i}, C_{r_i} , when they are wound, are equal to the negative time-derivatives of l_i, l_{r_i} , respectively. Using Eq. (3), the associated constraints on the joint velocities can be obtained as:

$$\dot{C}_{l_i} \in [-\dot{l}_{\max}, \dot{l}_{\max}] \implies -\dot{l}_i \in [-\dot{l}_{\max}, \dot{l}_{\max}] \implies -\frac{\dot{l}_{\max}}{Z_{l_i}} \leq \dot{\alpha}_i \leq \frac{\dot{l}_{\max}}{Z_{l_i}} \quad (4)$$

$$\dot{C}_{r_i} \in [-\dot{l}_{\max}, \dot{l}_{\max}] \implies -\dot{l}_{r_i} \in [-\dot{l}_{\max}, \dot{l}_{\max}] \implies -\frac{\dot{l}_{\max}}{-Z_{r_i}} \leq \dot{\alpha}_i \leq \frac{\dot{l}_{\max}}{-Z_{r_i}} \quad (5)$$

for $i = 1, 2$. The velocity of cable C_l (see Fig. 2, right) is $-(\dot{l}_1 + \dot{l}_2)$, leading to:

$$\dot{C}_l \in [-\dot{l}_{\max}, \dot{l}_{\max}] \implies -\dot{l}_{\max} \leq (Z_{l_1} \dot{\alpha}_1 + Z_{l_2} \dot{\alpha}_2) \leq \dot{l}_{\max} \quad (6)$$

For the 4-cable actuation scheme, the constraints in Eqs. (4) and (5) apply simultaneously, resulting in a total of eight constraints. For the 3-cable scheme, there are only six constraints defined by Eqs. (5) and (6). As an illustration, these constraints are shown in Fig. 3a (resp. Fig. 3b) for the 4-cable (resp. 3-cable) scheme, when the manipulator is at $(\alpha_1, \alpha_2) = (-1.65, 1.18)$ radians. The region respecting the constraints formed by the left cables (Eqs. (4), (6)) is shown

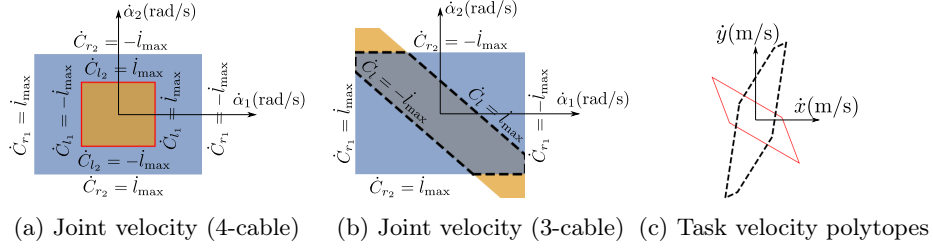


Fig. 3: Joint velocity polytope and task velocity polytope for the 4-cable (red continuous) and 3-cable (black dashed) schemes at $(\alpha_1, \alpha_2) = (-1.65, -1.18)$ rad.

in orange shade and by the right cables (Eq. (5)) in blue shade. The polytope that lies at the intersection of all the constraints represents the set of feasible joint velocities and is referred to as the joint velocity polytope. This polytope is highlighted by red continuous line for the 4-cable scheme and by black dashed line for the 3-cable scheme. This style is followed throughout the paper.

The corresponding polytope in the task velocity space (\dot{x}, \dot{y}) can be obtained by mapping the vertices of joint velocity polytope using the Jacobian matrix in Eq. (2). The task velocity polytopes for the two actuation schemes are superimposed in Fig. 3c. Interestingly, the polytope of the 3-cable scheme is larger, and its direction of maximum velocity is nearly perpendicular to its counterpart.

5 Static force analysis

The equation of static equilibrium for the 2-X manipulator can be written as:

$$\mathbf{J}^\top \mathbf{f} + \mathbf{G} = \mathbf{F} \quad (7)$$

where \mathbf{J} is the Jacobian matrix defined in Eq. (2), $\mathbf{f} = [f_x, f_y]^\top$ represents the forces applied by the robot end-effector on the environment, $\mathbf{G} = [G_1, G_2]^\top$ denotes the wrench due to the springs and gravity effects, and $\mathbf{F} = [F_1, F_2]^\top$ is the wrench applied by the cables, which depends on the actuation scheme.

For the 4-cable scheme, the cables C_{l_i}, C_{r_i} apply forces F_{l_i}, F_{r_i} on the i^{th} joint, respectively. Thus, the actuation wrench components are given by $F_i = Z_{l_i} F_{l_i} + Z_{r_i} F_{r_i}$, $i = 1, 2$ (see [8]), which can be written component-wise as:

$$\begin{bmatrix} J_{11} & J_{21} \\ J_{12} & J_{22} \end{bmatrix} \begin{bmatrix} f_x \\ f_y \end{bmatrix} + \begin{bmatrix} G_1 \\ G_2 \end{bmatrix} = \begin{bmatrix} Z_{l_1} F_{l_1} + Z_{r_1} F_{r_1} \\ Z_{l_2} F_{l_2} + Z_{r_2} F_{r_2} \end{bmatrix} \quad (8)$$

The limits on actuation forces shall be imposed as: $F_{l_i}, F_{r_i} \in [F_{\min}, F_{\max}]$ with numerical values $F_{\min} = 5$ N, $F_{\max} = 155$ N. Recalling that $Z_{l_i} > 0$ and $Z_{r_i} < 0$, the lower (resp. upper) bound of the actuation wrench F_i occurs when $F_{l_i} = F_{\min}, F_{r_i} = F_{\max}$ (resp. $F_{l_i} = F_{\max}, F_{r_i} = F_{\min}$). Thus, from Eq. (8), the following inequalities must hold:

$$Z_{l_i} F_{\min} + Z_{r_i} F_{\max} - G_i \leq (J_{1i} f_x + J_{2i} f_y) \leq Z_{l_i} F_{\max} + Z_{r_i} F_{\min} - G_i \quad (9)$$

for $i = 1, 2$. The region in the task force space (f_x, f_y) that satisfies these four conditions represents the force polytope for the 4-cable scheme. This is shown by the red continuous boundary for an example in Fig. 4.

In the 3-cable scheme, the side-routed cable C_l applies the same force F_l on the left side of both the joints (see Fig. 2, right), while the cable C_{r_i} applies a force F_{r_i} only on the i^{th} joint. Thus, the actuation wrench components are given by $\Gamma_i = Z_{l_i} F_l + Z_{r_i} F_{r_i}$. The associated equilibrium equation resembles the one in Eq. (8), with F_{l_1}, F_{l_2} replaced by F_l . Thus, proceeding in a similar manner, one obtains the same conditions in Eq. (9) for the 3-cable scheme also. Additionally, the constraints due to coupling of the side-routed cable C_l must also be imposed. This is obtained by firstly eliminating F_l from the two equilibrium equations:

$$J'_{11} f_x + J'_{21} f_y + G' = Z'_{l_1} F_{r_2} + Z_{r_1} F_{r_1} \quad (10)$$

where $J'_{i1} = \left(J_{i1} - \frac{Z_{l_1}}{Z_{l_2}} J_{i2} \right)$, $i = 1, 2$, $G' = \left(G_1 - \frac{Z_{l_1}}{Z_{l_2}} G_2 \right)$, $Z'_{l_1} = - \left(\frac{Z_{l_1}}{Z_{l_2}} Z_{r_2} \right)$. It can be shown that $Z'_{l_1} > 0$ in the above equation. Thus, the wrench bounds can be obtained as above, and the final conditions on (f_x, f_y) are:

$$Z'_{l_1} F_{\min} + Z_{r_1} F_{\max} - G' \leq J'_{11} f_x + J'_{21} f_y \leq Z'_{l_1} F_{\max} + Z_{r_1} F_{\min} - G' \quad (11)$$

The force polytope for the 3-cable scheme lies at the intersection of all the six conditions in Eqs. (9) and (11), as illustrated by the dashed boundary in Fig. 4.

Evidently, the force polytope of 3-cable scheme lies inside that of the 4-cable scheme, as it satisfies two additional conditions in Eq. (11). Thus, it can be concluded that the 4-cable actuation scheme permits the end-effector to apply more forces than the 3-cable scheme. From Fig. 4, it is observed that the force polytopes are off-centered w.r.t. the origin. This is an effect of gravity and springs.

6 Global performance inside the task space

The objective of this section is to use the velocity and force polytopes defined above, to assess the performance of the manipulator in the task space. In order to do this, it is firstly necessary to qualify the points (x, y) in the task space, to define a *workspace* for this manipulator. Several such definitions exist in the literature of cable-driven robots, e.g., wrench-closure workspace [6], wrench-feasible workspace [8]. In this study, a stable wrench-feasible workspace will be used. It is defined as the set of points (x, y) that can be reached by the end-effector, while satisfying the conditions of static equilibrium (only under self-weight), stability, and the bounds on actuation forces of the cables. It can be computed by a scanning method analogous to the one used in [8]. The details are not discussed here due to lack of space. A plot of this workspace is shown in Figs. 5 and 6 for the 4-cable (left) and 3-cable (right) schemes. As expected, the workspace obtained for the 4-cable scheme is larger than that of the 3-cable scheme.

Four points: P_1, P_2, P_3, P_4 (see Fig. 5) that are common to the workspaces of 4-cable and 3-cable actuation schemes have been chosen, to compare their

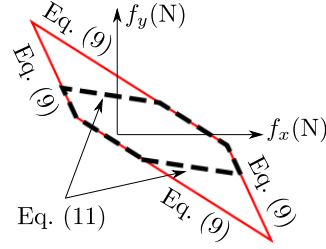


Fig. 4: Force polytopes and associated constraints of the 4-cable (red continuous) and 3-cable (black dashed) schemes at $(\alpha_1, \alpha_2) = (-1.65, -1.18)$ rad.

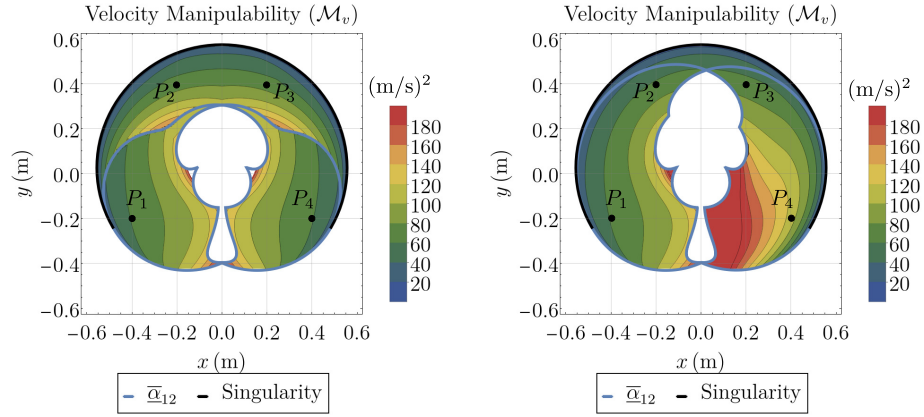


Fig. 5: Contour plot of velocity manipulability index inside the stable wrench-feasible workspace for the 4-cable (left) and 3-cable (right) actuation schemes.

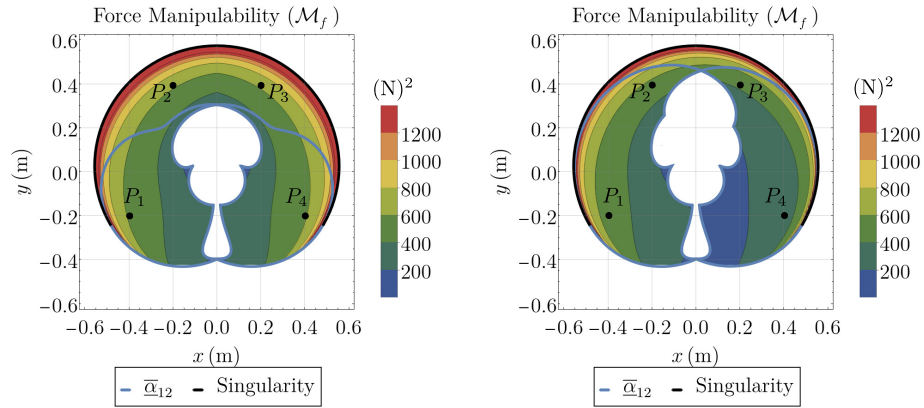


Fig. 6: Contour plot of force manipulability index inside the stable wrench-feasible workspace for the 4-cable (left) and 3-cable (right) actuation schemes.

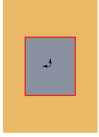


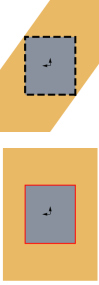


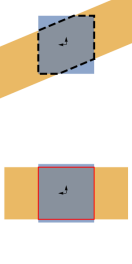
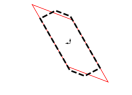
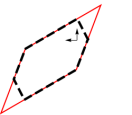
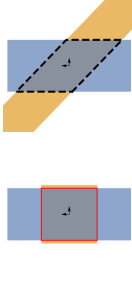
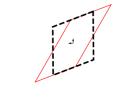
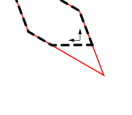
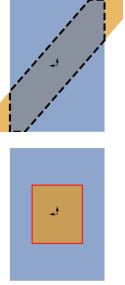
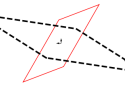
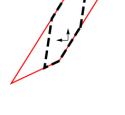
velocity and force performance locally. The velocity and force polytopes are visualized at these points in Table 1. In order to quantify the size and shape of these polytopes, two performance measures, namely, manipulability index (\mathcal{M}) and condition index, have been introduced in [4]. In this paper, the inverse of the condition index (κ) will be used instead of the condition index, as it is a bounded measure. Geometrically, the manipulability index measures the surface area of the polytope and the inverse condition index is the ratio of maximum performance (velocity/force) that can be achieved in *all* directions to the maximum performance inside the polytope. The distribution of velocity and force manipulability indices have been plotted for the two schemes inside their workspaces in Figs. 5 and 6, respectively. When there is more than one feasible configuration for the manipulator, the one that results in maximum performance measure is chosen. From these plots and Table 1, the following observations can be made:

- The velocity polytopes are identical at point P_1 , since the active constraints on the joint velocities are formed only by the cables C_{r_1}, C_{r_2} in both cases. Consequently, the velocity manipulability indices (\mathcal{M}_v) are also equal. But, for the 3-cable scheme, it is slightly lower at P_2 , equal at P_3 (with different polytope shape), and significantly greater at P_4 . This can also be verified from the contour plots in Fig. 5, where the distribution is nearly the same on the left half of the workspaces, but the value is significantly greater (about 1.53 times on average) on the right half for the 3-cable scheme.
- The velocity inverse condition index (κ_v) is greater for the 3-cable scheme at (P_2, P_3, P_4) . Inside the workspace, $(\kappa_v)_4 \in [0, 0.5]$ (4-cable) and $(\kappa_v)_3 \in [0, 0.7]$ (3-cable). Its distribution is not shown here due to lack of space.
- The force manipulability (\mathcal{M}_f) must be necessarily greater for the 4-cable scheme as the force polytope of 3-cable scheme must be contained inside that of the 4-cable one (see Section 5). The difference $((\mathcal{M}_f)_4 - (\mathcal{M}_f)_3)$ increases as one moves from P_1 to P_4 . From Fig. 6, it is found that \mathcal{M}_f is significantly lower (about 1/1.56 times on average) for the 3-cable scheme on the right half of the workspace, converse to that of velocity manipulability.
- The force inverse condition index (κ_f) is low, in general, for both the actuation schemes, due to the off-centered position of the polytopes. There is only a small difference in its value between the two schemes in (P_1, \dots, P_4) . Inside the workspace $(\kappa_v)_4 \in [0, 0.14]$ (4-cable) and $(\kappa_v)_3 \in [0, 0.18]$ (3-cable).

7 Conclusion

The instantaneous velocity and static force analysis have been performed for the 2-X tensegrity manipulator for two different cable actuation schemes. The first scheme involves four cables, while the second one involves only three. Practical limits have been considered on the cable velocities and the actuation forces. The effect of these limits on the end-effector velocity and force-application capabilities have been studied for the two actuation schemes, in terms of polytopes.

Table 1: Comparison of velocity and force polytopes for 4-cable and 3-cable actuation schemes at discrete points in their workspaces. The joint velocity constraints imposed by the left cables ($C_{l_1}, C_{l_2}, C_{l_3}$) are shown in orange shade, and those imposed by the right cables (C_{r_1}, C_{r_2}) in blue shade, for both the schemes. The resulting polytopes obtained for the 4-cable (resp. 3-cable) scheme are shown in red continuous (resp. black dashed) boundary. Symbols $(\mathcal{M}_v, \kappa_v)$ and $(\mathcal{M}_f, \kappa_f)$ denote (manipulability, inverse condition index) for velocity and force polytopes, respectively. A measure (\cdot) associated with 4-cable scheme is given by $(\cdot)_4$ and with 3-cable scheme by $(\cdot)_3$. All the numerical values have been rounded off to 2 decimal places.

Position [m]/ Configura- tion [rad]	Joint velocity polytopes ($\dot{\alpha}_1, \dot{\alpha}_2$) (4-cable) 	Task velocity polytopes (\dot{x}, \dot{y}) 	Task force polytopes (f_x, f_y) 	\mathcal{M}_v [(m/s) ²], \mathcal{M}_f [N ²] κ_v, κ_f [no units]
$P_1 =$ $(-0.4, -0.2);$ $(\alpha_1, \alpha_2) =$ $(1.65, 1.18)$				$(\mathcal{M}_v)_4 = 61.18, (\mathcal{M}_v)_3 = 61.18$ $(\kappa_v)_4 = 0.18, (\kappa_v)_3 = 0.18$ $(\mathcal{M}_f)_4 = 579.68, (\mathcal{M}_f)_3 = 518.45$ $(\kappa_f)_4 = 0.04, (\kappa_f)_3 = 0.04$
$P_2 =$ $(-0.2, 0.4);$ $(\alpha_1, \alpha_2) =$ $(-0.2, 1.57)$				$(\mathcal{M}_v)_4 = 67.35, (\mathcal{M}_v)_3 = 63.26$ $(\kappa_v)_4 = 0.25, (\kappa_v)_3 = 0.35$ $(\mathcal{M}_f)_4 = 657.14, (\mathcal{M}_f)_3 = 549.08$ $(\kappa_f)_4 = 0.09, (\kappa_f)_3 = 0.12$
$P_3 =$ $(0.2, 0.4);$ $(\alpha_1, \alpha_2) =$ $(0.2, -1.57)$				$(\mathcal{M}_v)_4 = 67.35, (\mathcal{M}_v)_3 = 67.35$ $(\kappa_v)_4 = 0.25, (\kappa_v)_3 = 0.54$ $(\mathcal{M}_f)_4 = 657.14, (\mathcal{M}_f)_3 = 443.68$ $(\kappa_f)_4 = 0.09, (\kappa_f)_3 = 0.06$
$P_4 =$ $(0.4, -0.2);$ $(\alpha_1, \alpha_2) =$ $(-1.65, -1.18)$				$(\mathcal{M}_v)_4 = 61.18, (\mathcal{M}_v)_3 = 109.71$ $(\kappa_v)_4 = 0.18, (\kappa_v)_3 = 0.22$ $(\mathcal{M}_f)_4 = 579.68, (\mathcal{M}_f)_3 = 316.38$ $(\kappa_f)_4 = 0.04, (\kappa_f)_3 = 0.05$

A comparative study has been carried out between the velocity and force polytopes of the 4-cable and 3-cable schemes, in terms of their manipulability and inverse condition indices. It is observed that the velocity manipulability of the 3-cable scheme is significantly larger than its counterpart on the right half of the workspace. However, its force manipulability is less than that of the 4-cable scheme throughout its workspace, and significantly lower on the right half. The velocity inverse condition index is greater for the 3-cable scheme, but there is no significant difference in the force inverse condition index between the two schemes. In summary, the 3-cable scheme has a smaller stable wrench-feasible workspace, lesser force capabilities, but larger velocity capabilities in some parts of the workspace. In the future, these velocity and force indices will be used to design tensegrity manipulators for manipulation and machining applications.

References

1. Gouttefarde, M., Daney, D., Merlet J.: Interval-Analysis-Based Determination of the Wrench-Feasible Workspace of Parallel Cable-Driven Robots. *IEEE Transactions on Robotics*, 27(1), 1-13 (2011)
2. Bouchard, S., Gosselin, C., Moore, B.: On the Ability of a Cable-Driven Robot to Generate a Prescribed Set of Wrenches. *ASME J. Mechanisms Robotics* 2(1) (2010)
3. Lessanibahri, S., Gouttefarde, M., Stéphane Caro, S., Cardou, P.: Twist feasibility analysis of cable-driven parallel robots. In: *Cable-driven parallel robots*, pp. 128-139, Cham: Springer (2018)
4. Lee, J.: A study on the manipulability measures for robot manipulators. In: *Proceedings of the 1997 IEEE/RSJ International Conference on Intelligent Robot and Systems, IROS '97*, vol. 3, pp. 1458-1465 (1997)
5. Rezazadeh, S., Behzadipour, S.: Workspace Analysis of Multibody Cable-Driven Mechanisms. *ASME J. Mechanisms Robotics* 3(2) (2011)
6. Ramadoss, V., Lau, D., Zlatanov, D., Zoppi, M.: Analysis of Planar Multilink Cable Driven Robots Using Internal Routing Scheme. In: *Proceedings of the ASME 2020 International Design Engineering Technical Conferences and Computers and Information in Engineering Conference* (2020)
7. Mustafa, S. K., Agrawal, S. K.: On the Force-Closure Analysis of n-DOF Cable-Driven Open Chains Based on Reciprocal Screw Theory. *IEEE Transactions on Robotics* 28(1), 22-31 (2012)
8. Furet, M., Wenger, P.: Kinetostatic analysis and actuation strategy of a planar tensegrity 2-X manipulator. *ASME J. Mechanisms Robotics* 11(6) (2019)
9. Hamon, A., Aoustin, Y., Caro, S.: Two walking gaits for a planar bipedal robot equipped with a four-bar mechanism for the knee joint. *Multibody System Dynamics* 31(3), 283-307 (2014)
10. Fasquelle, B., Khanna, P., Chevallereau, C., Chablat, D., Creusot, D., Jolivet, S., Lemoine, P., Wenger, P.: Identification and Control of a 3-X Cable-Driven Manipulator Inspired From the Bird's Neck. *ASME J. Mechanisms Robotics* 14(1) (2022)
11. Wenger, P., Furet, M.: Kinematic Analysis of a Planar Manipulator with Antiparallelogram Joints and Offsets. In: *Proceedings of ARK 2020*, J. Lenarčič and B. Siciliano Eds., pp. 319-326, Cham: Springer Int. Publishing (2021)
12. Furet, M., van Riesen, A., Chevallereau, C., Wenger, P.: Optimal design of tensegrity mechanisms used in a bird neck model. In: *EuCoMeS 2018*, B. Corves, P. Wenger, and M. Hüsing Eds., pp. 365-375. Cham: Springer Int. Publishing (2019)